Journal of Electron Spectroscopy and Related Phenomena 200 (2015) 49–63

Contents lists available at ScienceDirect

Journal of Electron Spectroscopy and Related Phenomena

journal homepage: www.elsevier.com/locate/elspec

Soft X-ray spectromicroscopy and ptychography

Adam P. Hitchcock*

Dept of Chemistry and Chemical Biology, McMaster University, Hamilton, ON, L8S 4M1, Canada

ARTICLE INFO

Article history:
Available online 3 June 2015

Keywords:
Soft X-ray absorption
STXM
SPEM
XPEEM
TXM
Ptychography

ABSTRACT

Instrumentation and current capabilities of soft X-ray (50–2000 eV) spectromicroscopy are outlined with examples from recently published and some new work. Four common techniques are treated—transmission X-ray microscopy (TXM), scanning transmission X-ray microscopy (STXM), X-ray photoemission electron microscopy (XPEEM) and scanning photoemission microscopy (SPEM). I also present a fifth, emerging technique, that of soft X-ray spectro-ptychography which has significantly improved spatial resolution and provides new contrast mechanisms. Perspectives for near future (5–10 years) evolution of soft X-ray spectromicroscopy are outlined based on current trends and instrumentation under development.

1. Introduction

Spectromicroscopy refers to methods in which imaging and spectroscopic analysis are used in a balanced way. There are many types of spectromicroscopy since almost all possible forms of imaging and spectroscopy can be combined with sufficient ingenuity. This article restricts its scope to those methods in which tunable energy soft X-rays ($50 < h\nu < 3000$ eV, typically from a synchrotron light source) are used for spectrally sensitive imaging, based on systematic changes of the incident photon energy and/or polarization properties of the soft X-rays, and/or the properties of primary or secondary particles (X-rays, electrons, visible photons, ions, etc) produced by photoionization. There are four common types of soft X-ray spectromicroscopy: scanning transmission X-ray microscopy (STXM), scanning photoelectron microscopy (SPEM), full field transmission X-ray microscopy (TXM) and X-ray photoemission electron microscopy (XPEEM). Fig. 1 presents schematics of these techniques. In addition, this article describes recently developed soft X-ray ptychography, a STXM-based form of coherent diffraction imaging (CDI) which is making dramatic improvements in spatial resolution and spectral sensitivity. All five methods have the potential to perform spectromicroscopy based on near edge X-ray absorption fine structure (NEXAFS) contrast. SPEM, and XPEEM, with addition of an electron dispersive analyzer, can also perform spectromicroscopy based on photoelectron spectroscopy contrast. SPEM and STXM systems can and have been equipped with silicon drift detectors to allow X-ray fluorescence spectroscopy and XRF-yield NEXAFS detection.

There are closely related spectromicroscopy techniques using tunable hard X-rays but the spectral sensitivity typically is restricted to elemental characterization. NEXAFS in the soft X-ray spectral region has incredible sensitivity to the detailed electronic structure needed to do full speciation – identification of individual chemical species – which is central to the interests of the readers of the Journal of Electron Spectroscopy and Related Phenomena. The soft X-ray region also includes the water window (200–520 eV) which facilitates studies of samples in aqueous environments. Furthermore the spectral resolution and the routinely available spatial resolution (as well as the record spatial resolution) is better in the soft X-ray than in the hard X-ray region.

This article is not intended to cover all of this large and rapidly expanding field, but rather to outline the four main types of instrumentation, illustrate their performance with state-of-the-art instruments, and provide a perspective on expected near future developments. Reviews covering all four types of soft X-ray spectromicroscopy include those by Hitchcock in 2012 [1], Ade and Hitchcock in 2008 [2]. Bauer [3] recently authored a book on low energy surface microscopy which gives comprehensive coverage of XPEEM and some treatment of SPEM. Günther et al. [4] published a comprehensive review of photoelectron microscopy (SPEM, XPEEM) applied to surface and materials science. Howells et al. [5] reviewed all types of zone plate based microscopy (STXM, TXM, SPEM) with emphasis on the fundamental physics and X-ray optics. Kaulich et al. [6] recently gave an overview of

* Tel.: +1 905 525 9140 24749; fax: +1 905 521 2773.
E-mail address: aph@mcmaster.ca

http://dx.doi.org/10.1016/j.elspec.2015.05.013
0368-2048/

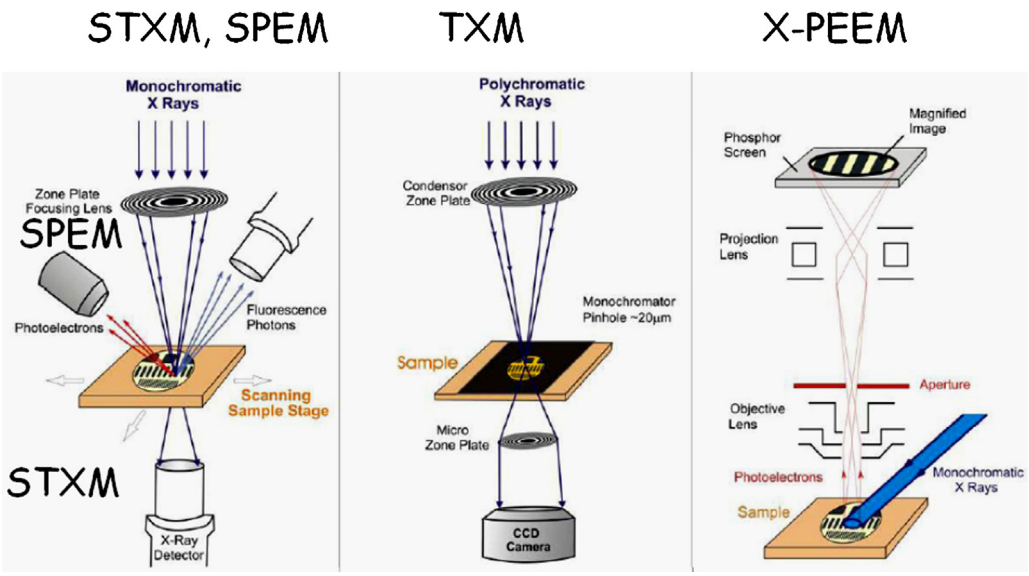

Fig. 1. Overview of the four common types of soft X-ray spectromicroscopy: scanning transmission X-ray microscopy (STXM), scanning transmission X-ray microscopy (SPEM), full field transmission (TXM) and full field X-ray photoemission electron microscopy (X-PEEM).

instrumentation and applications for X-ray-in/X-ray-out microscopies (STXM with both transmission and fluorescence detection, as well as ptychography). Falcone et al. [7] presented a review intended for non-experts that surveys the whole field of X-ray microscopy, including laboratory and free-electron-laser methods. Older but still authoritative reviews of the field include the book by David Attwood [8] and the review of biological applications by Kirz et al. [9]. A colorful and informative review of the history of the development of soft X-ray microscopy was recently published by Kirz and Jacobsen [10]. The last time a comprehensive treatment of soft X-ray microscopy was presented in this journal was the Special Issue on Soft X-ray Microscopy, Volume 84 (1997). There is an article in this volume by Carpenter et al. [11] which provides a review and perspective on the complementary methods of soft X-ray resonant and non-resonant scattering. A review article focusing on 3D chemical imaging by soft X-ray spectro-tomography has recently been published by Schmid et al. [12]. I also note recent reviews of hard X-ray spectromicroscopy [13] and tomography [14].

This article is organized as follows. Section 2 gives an overview of soft X-ray spectromicroscopy instrumentation using the highest performing instruments of each of the four classes as examples. This is followed by a set of recent scientific examples using each of the 4 types, chosen to illustrate state-of-the-art capabilities. Section 4 focuses on the emerging technique of soft X-ray ptychography (note hard X-ray ptychography is relatively well developed and is extensively covered in a recent review [13]). Section 4 describes the ptychography method and presents some recently published results on lithium battery materials and new results on biological magnetism. The final section provides my perspective on near future directions, focusing on new capabilities that are now, or will soon be, possible due to improvements to instrumentation. Emerging applications of soft X-ray spectromicroscopy are also noted.

2. Current instrumentation and facilities

Table 1 is a list of the soft X-ray spectromicroscopy facilities around the world. It lists both existing operational systems and also those under construction or commissioning. Fig. 2a is a temporal display of the evolution of the numbers of each of the 4 types of instruments at synchrotron facilities, as well as their productivity (Fig. 2b). The annual numbers of publications from each type of microscopy is derived from a bibliography of soft X-ray spectromicroscopy that I maintain, which is available as a supplemental material to this article. Periodic updates are available at http://unicorn.chemistry.mcmaster.ca/xrm-biblio/xrm_bib.html. While I have done the best I could to bring this document up to date with

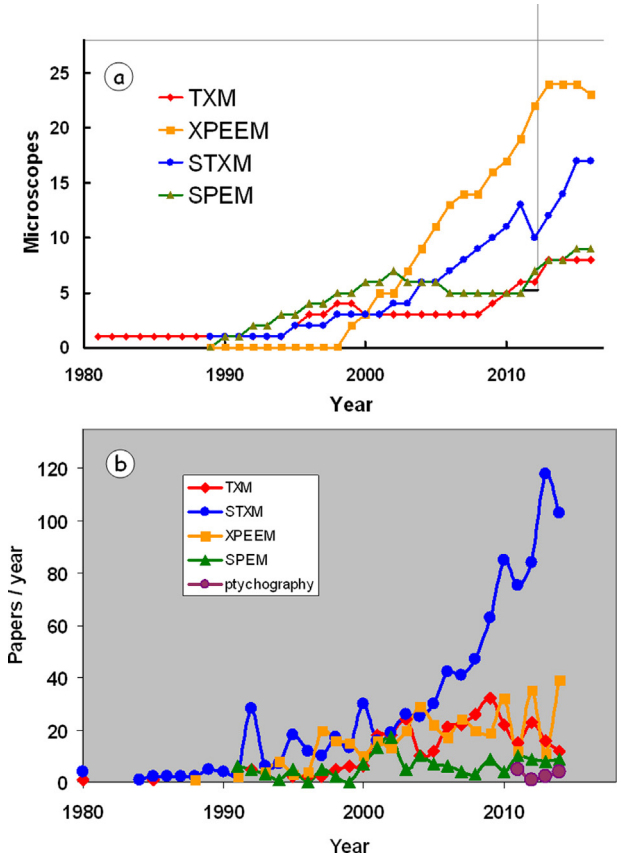

Fig. 2. Overview of (a) the growth internationally in numbers of soft X-ray microscopes, and (b) scientific output of the 4 types of soft X-ray microscopes. Publications based on soft X-ray ptychography are just starting to appear but this technique is expected to develop rapidly.

Table 1
Soft X-ray spectromicroscopy facilities at synchrotron light sources.

Type	Facility	Name	City	Country	Source	E-range (eV)	1st image	Status	Comments
TXM	Alba	Mistral	Barcelona	Spain	BM	270–2600	2013	Operating	Xradia
TXM	ALS	XM1	Berkeley	USA	BM	250–900	1995	Operating	
TXM	ALS	XM2 (NCXT)	Berkeley	USA	BM	250–6000	2009	Operating	
TXM	Astrid	XRM	Aarhus	Denmark	BM	500	1998	Operating	
TXM	Bessy-I		Berlin	Germany	BM	500	1989	Ended 1999	
TXM	Bessy-II	U41-TXM	Berlin	Germany	Und-L	250–600	2010	Operating	
TXM	Diamond	B24 cryo-TXM	Harwell	UK	BM	250–2500	2013	Operating	Xradia
TXM	NSRL	TXM	Hefei	China	BM	500	2011	Operating	Xradia
TXM	Ritsumeikan	BL12	Kyoto	Japan	BM	500	1996	Operating	
XPEEM	Alba	Circe	Barcelona	Spain	EPU	100–2000	2013	Construction	Elmitec
XPEEM	ALS	PEEM-2	Berkeley	USA	BM	175–1500	1999	Ended 2011	custom electrostatic
XPEEM	ALS	PEEM-3	Berkeley	USA	EPU	150–2000	2009	Operating	custom electrostatic
XPEEM	APS	BL 4IDC	Argonne	USA	Und-L	500–2500	2012	Operating	Omicron, Elmitec
XPEEM	Bessy-II	SMART	Berlin	Germany	EPU	100–1800	2004	Operating	custom
XPEEM	Bessy-II	UE49	Berlin	Germany	EPU	100–1800	2006	Operating	Elmitec
XPEEM	Bessy-II	UE56	Berlin	Germany	EPU	100–1800	2012	Commissioning	Specs
XPEEM	CLS	CaPeRS	Saskatoon	Canada	EPU	130–2500	2003	Operating	Elmitec
XPEEM	Diamond	IO6	Chilton	UK	EPU	80–2100	2012	Operating	Elmitec
XPEEM	Elettra	BL 1.2 L	Trieste	Italy	EPU	50–1000	1999	Operating	Elmitec SPELEEM
XPEEM	Hi-SOR	BL-5	Hiroshima	Japan	BM	50–300	2006	Operating	
XPEEM	MAXlab	1311	Lund	Sweden	Und-L	100–1400	2011	Operating	Elmitec
XPEEM	NSLS-I	U5UA	Brookhaven	USA	Und-L	15–150	2006	Ended 2015	
XPEEM	NSRRC	BL05B2	Hinschu	Taiwan	EPU	60–1400	2002	Operating	Omicron
XPEEM	PLS	4B1	Pohang	Korea	BM	200–1000	2000	Operating	
XPEEM	PF	BL 19B	Tsukuba	Japan	BM	50–150	2001	Operating	
XPEEM	PF	BL 27A	Tsukuba	Japan	BM	50–150	2010	Operating	STAIB Spector
XPEEM	SLS	SIM	Villigen	Switzerland	EPU	90–1200	2005	Operating	
XPEEM	Soleil	Tempo	Saint-Aubin	France	EPU	50–1500	2008	Operating	Focus, Omicron
XPEEM	Soleil	Hermes	Saint-Aubin	France	EPU	250–1500	2013	Operating	Elmitec, PEEM/LEEM
XPEEM	SRLI	BL4	Nakon Ratchasima	Thailand	BM	40–1040	2015	Commissioning	
XPEEM	Spring-8	BL25SU	Hyogo	Japan	EPU	220–2000	2001	Operating	Elmitec
XPEEM	Spring-8	BL17SU	Hyogo	Japan	EPU	300–1800	2005	Operating	SPELEEM
XPEEM	SRC	Sphinx	Stoughton	USA	Und-L	70–2000	2004	Ended 2013	now at APS
XPEEM	SSLS	SINS	Singapore	Singapore	BM	50–1200	2011	Operating	Focus-PEEM
XPEEM	SSRF	BL08U1	Shanghai	China	Und-L	50–1200	2012	Operating	Elmitec
STXM	ALS	7.0.1	Berkeley	USA	Und-L	100–1200	1995	Ended 2001	
STXM	ALS	5.3.2.2	Berkeley	USA	BM	250–750	2001	Operating	
STXM	ALS	11.0.2	Berkeley	USA	EPU	100–2000	2002	Operating	
STXM	ALS	5.3.2.1	Berkeley	USA	BM	250–2500	2011	Operating	
STXM	Australian SR		Melbourne	Australia	Und-L	100–2000	2014	Commissioning	Xradia/APS upgraded
STXM	Bessy -II	old-STXM	Berlin	Germany	BM	250–600	2004	Ended 2011	
STXM	Bessy-II	MAXYMUS	Berlin	Germany	EPU	250–1500	2008	Operating	Bruker
STXM	CLS	10ID1	Saskatoon	Canada	EPU	130–2500	2006	Operating	custom
STXM	CLS	10ID1	Saskatoon	Canada	EPU	130–2500	2015	Commissioning	custom, cryo-STXM
STXM	Diamond	I08	Harwell	UK	EPU	250–2500	2015	Construction	Bruker
(S)TXM	Elettra	Twin-mic	Trieste	Italy	Und-L	250–2000	2002	Operating	
STXM	UVSOR	BL4U	Okazaki	Japan	Und-L	50–800	2013	Operating	Bruker
STXM	NSLS	X1A	Upton	USA	Und-L	250–1000	1989	Ended 2000	
STXM	NSLS	X1A	Upton	USA	Und-L	250–1000	1998	Ended 2011	cryo-STXM
STXM	NSLS	X1A	Upton	USA	Und-L	250–1000	2004	Ended 2011	STXM IV
STXM	NSRRC	BL09A1	Hinschu	Taiwan	Und	60–1500	2017	Construction	
STXM	PLS	nanoscopy	Pohang	Korea	EPU	100–2000	2014	Construction	Bruker
STXM	PF	Various BL	Tsukuba	Japan	BM	100–8000	2013	Operating	Atto-cube
STXM	SLS	PolLux	Villigen	Switzerland	BM	250–750	2006	Operating	Bruker
STXM	SLS	NanoXAS	Villigen	Switzerland	BM	270–1800	2009	Operating	custom
STXM	Soleil	Hermes	Saint-Aubin	France	EPU	250–1500	2015	Construction	Bruker
STXM	SSRF	SXS	Shanghai	China	EPU	200–2000	2011	Operating	Xradia
STXM	SSRL	13-1	Stanford	USA	EPU	250–1000	2010	Operating	Atto-cube based
SPEM	ALS	BL 7.0	Berkeley	USA	Und-L	90–1300	1996	Ended 2006	
SPEM	ALS	BL 11.0.2	Berkeley	USA	EPU	100–2000	2013	Commissioning	ambient pressure
SPEM	ALS	Maestro	Berkeley	USA	EPU	90–1300	2015	Commissioning	
SPEM	Elettra	BL 2.2 L	Trieste	Italy	Und-L	350–750	1994	Operating	
SPEM	Elettra	BL 3.2 L	Trieste	Italy	Und-L	27, 95	2000	Operating	Schwarzchild, nanoARPES
SPEM	MAX-lab	BL 31	Lund	Sweden	Und-L	15–150	1992	Operating	
SPEM	NSLS-I	X1A	Brookhaven	USA	Und-L	250–600	1990	Ended 2002	
SPEM	NSRRC	BL09A1	Hinschu	Taiwan	Und	250–1500	1998	Operating	
SPEM	PLS	8A1	Pohang	Korea	Und	20–2000	2002	Operating	
SPEM	Soleil	Antares	Saint-Aubin	France	EPU	50–1500	2012	Operating	
SPEM	Spring-8	BL07LSU	Hyogo	Japan	EPU	220–2000	2012	Operating	

the time I had available, in particular to identify all publications based on synchrotron soft X-ray spectromicroscopy, I am sure it is incomplete and possibly skewed in coverage. I welcome corrections and additions to the bibliography.

Full field transmission X-ray microscopy (TXM) was developed by Schmahl and co-workers at the BESSY I synchrotron in Berlin [15,16]. The present generation TXM at Bessy II (Fig. 3) is equipped with a full, high resolution monochromator and provides

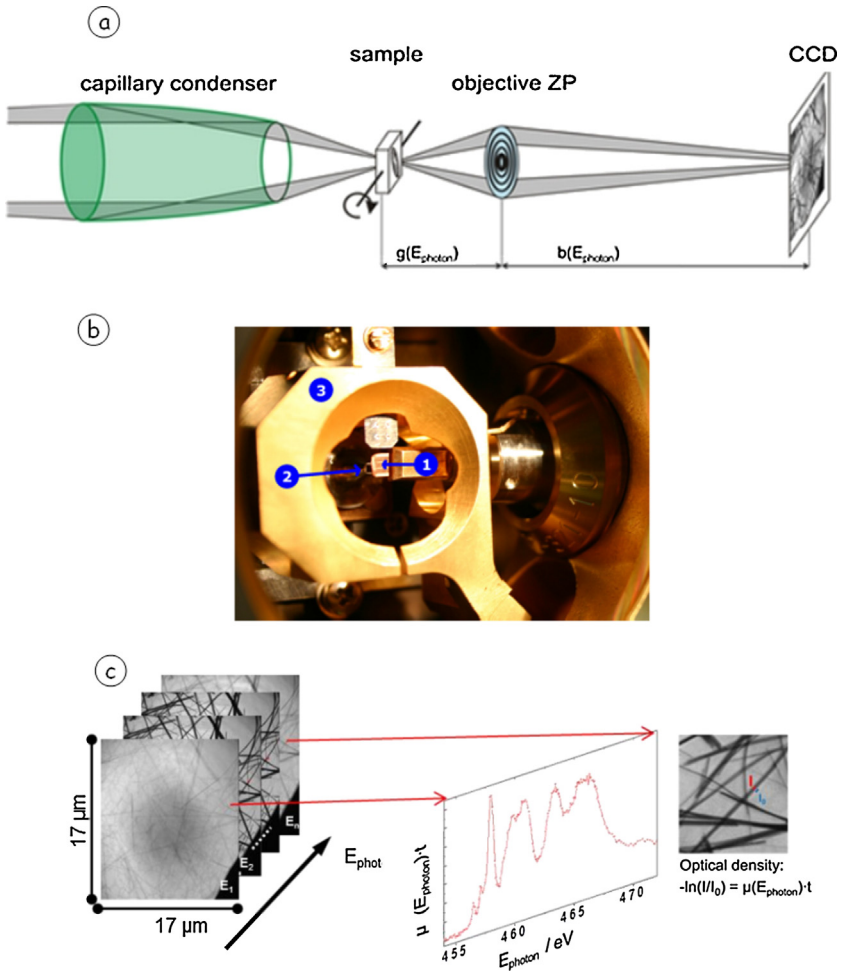

Fig. 3. (a) Schematic of the full field transmission X-ray microscope (TXM) at Bessy-II (Berlin). The beamline provides photons from 270–1500 eV, with a resolving power ($E/\Delta E$) >10000. Its record spatial resolution is 11 nm, the maximum field of view is 38 μm, and typical exposure times are 1 s [17]. (b) Photo of sample region (1) the cryogenic tomography sample holder. (2) X-ray objective, (3) cold trap. (c) Illustration of TXM-based spectromicroscopy, from multi-energy image sequence, to spectra and component maps (adapted from [17], open access).

full spectromicroscopy capabilities [18] as do the other soft X-ray TXMs equipped with monochromators at Alba [19] and Diamond. TXMs require incoherent illumination; otherwise there are Frsenel fringes at the boundaries of each object [5]. For systems without a monochromator such as XM-1 [19] and XM-2 [20] at the Advanced Light source (ALS), a large zone plate condenser is used to provide the optimum multi-directional (incoherent) illumination. In spectro-TXM systems (those with conventional monochromators) the X-ray beam delivered by the monochromator is too coherent and thus a rotating capillary optic (Fig. 3**a**) is used to degrade the coherence [21]. However, it is difficult to achieve uniform illumination in this way. Despite this, interesting spectromicroscopy data has been obtained as exemplified below. An outstanding feature of the Bessy-II spectro-TXM is that it is equipped with a cryo-tomography stage (Fig. 3**b**), modified from a transmission electron microscopy (TEM) stage.

Scanning transmission X-ray microscopy (STXM) using zone plate focusing was first demonstrated in 1980 by Sayre, Kirz and coworkers [22]. The first spectromicroscopy publication from STXM was that by Ade et al. in 1992 [23]. Fig. 4a is a photograph of the ambient-STXM [24] at the BL10ID1 spectromicroscopy facility at the Canadian Light source (CLS), which is able to operate in air, He or a low vacuum (~10^{-6} torr), Fig. 4b and c are the UHV enclosure and the interior mechanism of the cryo-STXM, which is presently under commissioning at the CLS. It will have clean, low contamination rate, near-UHV vacuum to enable cryo-spectro-tomography. A modified TEM eucentric stage and cryo-sample rotation system will be used, along with zone plate and order sorting aperture (OSA) scanning rather than the more conventional sample scanning.

Although photoemission electron microscopes (PEEM) with lab-based UV sources were developed in the 1930's, the first XPEEM instrument was that at the Synchrotron Radiation Centre (SRC) in Stoughton, WI built by Tonner and Harp [26]. There are now a number of commercial vendors of PEEM instruments designed to adapt to synchrotron facilities. Fig. 5 presents images of the Elmitec PEEM-3 instrument which is used at CLS, Soleil, Elettra, Diamond, Max-III, among other facilities. The configuration in Fig. 5a includes an energy analyzer which allows for energy resolved photoelectron spectroscopy and XPS-based spectromicroscopy, in addition to variation of the incident photon energy (NEXAFS spectral imaging). The CLS XPEEM is equipped with this type of energy analyzer. An upgrade is underway to add a second magnifying column to allow for rapid switching between NEXAFS and XPS imaging modes. Fig. 5b shows the motorized variant of the sample manipulator while Fig. 5c is a photo of the Elmitec sample holder, which is capable of heating to very high temperatures (>2000 °C) as well as liquid N_2 cooling. XPEEM systems are fully UHV systems. They are ideal for examining surface reactions carried out *in situ* although in many

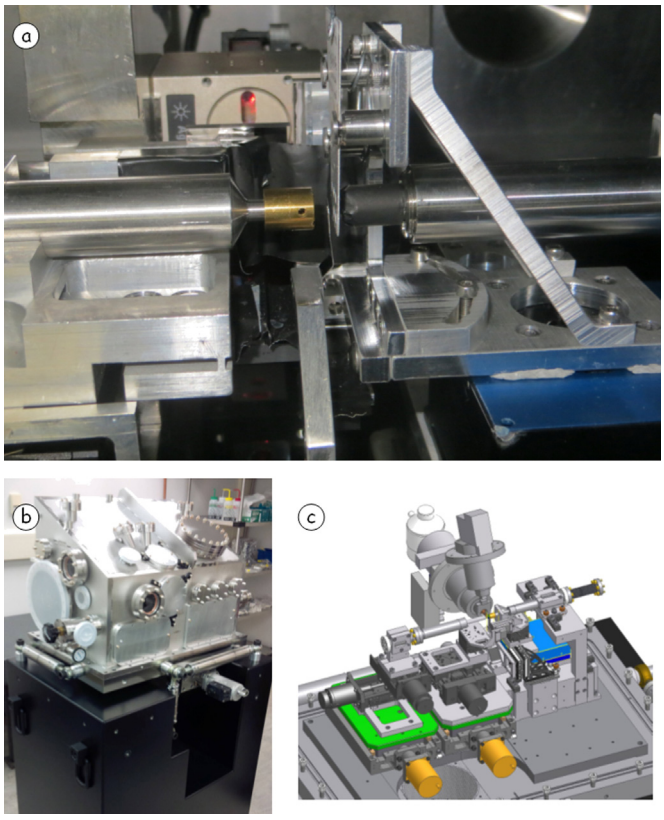

Fig. 4. (a) Photograph of the interferometer controlled ambient-STXM at the CLS 10ID1 beamline. (b) vacuum enclosure and granite support of the cryo-STXM presently under development at the CLS. (c) drawing of the stage system for the CLS cryo-STXM.

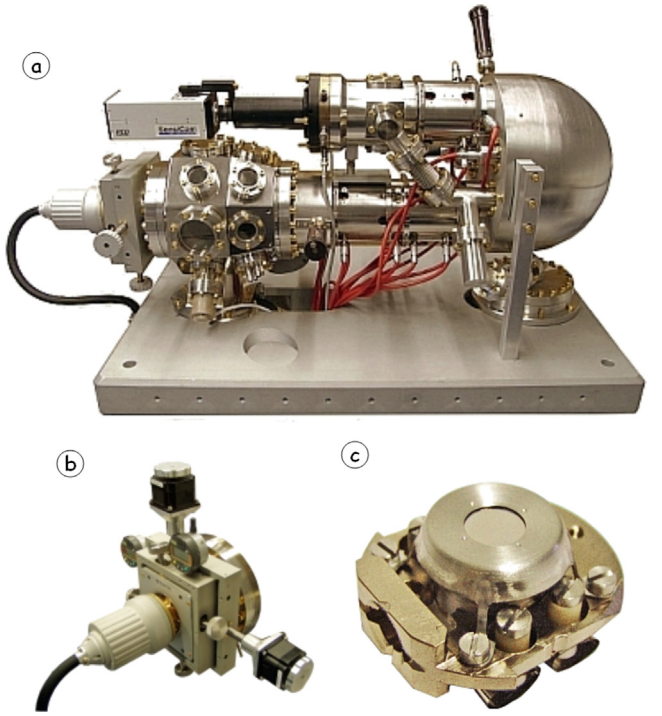

Fig. 5. (a) Photograph of the Elmitec PEEM-3 instrument equipped with an electron energy analyzer, which is similar to the present XPEEM at CLS 10ID1, (b) the manipulator, (c) the sample holder, equipped with heater, thermocouples etc.

cases they are also used as a near-surface materials analysis tool. Typically samples must be UHV-compatible (low outgassing), conducting and very flat, since field emission occurs from asperities due to the very high electric field (∼10 kV/mm) of the objective lens.

Scanning photoemission X-ray microscopy (SPEM) was first demonstrated by Ade et al. in 1991 [25]. SPEM is very challenging due to (i) the low intensity of the zone plate focused spot (10^7–10^9 ph/s in ∼100–500 nm), which is orders of magnitude weaker than normal photoemission spectroscopy systems used for angle resolved photoemission (ARPES), and (ii) the yield of at-energy photoelectrons is very low since they are produced only from the outermost ∼0.5 nm of the sample, and which are detected with modest efficiency, even with modern high efficiency lenses and 2D analyzers equipped with multi-channel detectors. Despite these challenges, productive and user-friendly SPEM facilities exist at Elettra, NSRRC, PLS, Soleil and others (see Table 1). With recent improvements in energy analyzer efficiency, high precision motion stages, and laser based interferometry, the most recent SPEM systems are able to perform sophisticated photoemission experiments such as band structure determination by angle-resolved PES at a spatial resolution below 100 nm (nano-ARPES). Fig. 6 is a set of images of the nano-ARPES SPEM system at the Antares beamline at the Soleil synchrotron [27]. This sophisticated beam line uses a variable line spacing, variable groove depth plane grating monochromator (VLS-VGD-PGM) and focusing optics pre- and post-monochromator, with the pre-zone plate beam concentrated using a double pseudo-Wolter optic. Despite having 7 optical surfaces (versus only 3 in e.g. the PGM beamlines ALS11.0.2 and CLS 10ID1) its photon flux, brightness and energy resolution are excellent. Antares uses very large zone plates to have a long working distance at relatively low X-ray energy, and very sophisticated interferometer controlled motion systems to achieve precise alignment of the focused beam and the sample at the focal point of the photoelectron energy analyzer. In many ways it sets the standard for state-of-the-art SPEM/nano-ARPES instrumentation.

3. Examples of recent soft X-ray spectromicroscopy research

3.1. Spectromicroscopy in TXMs

The parallel acquisition of full field TXM should make it the premier type of soft X-ray microscopy for 'bulk' studies since it can acquire images much faster than STXM. However, it is only in the last few years that TXMs have been developed at Bessy-II and Alba on beamlines equipped with modern dispersive monochromators, which are essential for high quality spectromicroscopy. Prior to that only very low resolution energy selection ($E/\Delta E \sim 100$) was available from the chromatic properties of the condenser zone plates and it was very difficult to do much more than elementally sensitive analysis. Fig. 7 presents the orientation dependent Ti 2p spectra of $NaTiO_x$ nanorods [28] obtained from two different nanorods with similar thickness. Understanding the electronic and geometric structure and the chemistry of titania nanomaterials is of great interest at present since these types of materials are being evaluated for possible use in gas sensors, photovoltaics, etc. They are also of fundamental interest since highly anisotropic nanostructured materials, such as $NaTiO_x$ nanorods offer good models to study the dependence of electrical, thermal transport and mechanical properties on directionality and size reduction. Without examining the Ti 2p spectra of individual $NaTiO_x$ nanotubes using polarized X-rays one might conclude the only aspects of interest are relatively subtle changes in the line shape, which is derived from the complex interplay of spin-orbit splitting (into

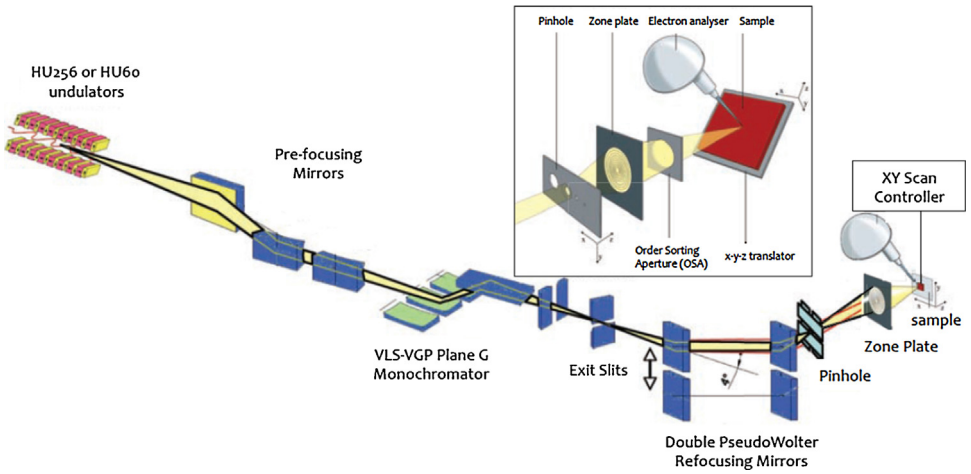

Fig. 6. Schematic of the Antares beamline at Soleil which features a scanning photoemission microscope (SPEM) specialized for angle resolved photoemission (nano-ARPES) [27] (open access).

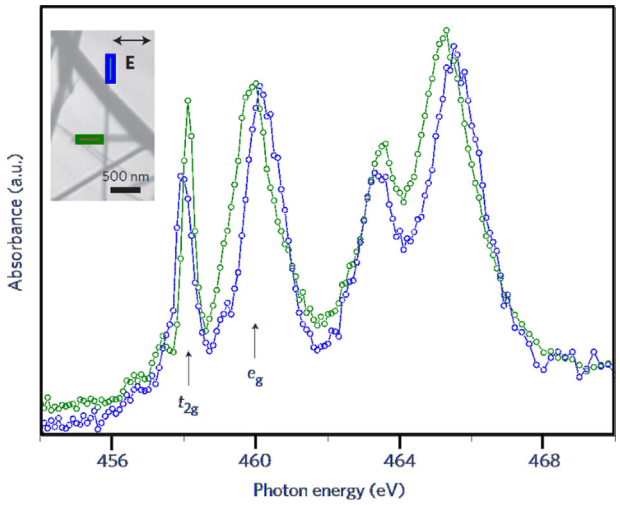

Fig. 7. Ti 2p spectra of two different $NaTiO_x$ nanorods, recorded with linear horizontal polarization using the full field TXM at BESSY II [28]. The inset figure is a transmission image with the two nanorods identified (figure adapted from [28], used with permission, Rights Link license 3570550952215).

$2p_{3/2}$ and $2p_{1/2}$), ligand field splitting (t_{2g}, e_g), atomic multiplet effects, and covalent metal-ligand interactions. However the pioneering TXM spectromicroscopy study by Guttmann et al. [28] revealed a subtle but significant polarization dependence (linear dichroism) which is manifested as an apparent shift in peak positions (Fig. 7). Although a complete spectral determination awaits detailed high level calculations, the present understanding is that the shifts are only apparent, and arise from the overlapping dichroism of individual, unresolved transitions that combine to form the complex multi-line spectrum. Other TXM spectromicroscopy include studies of thin graphite flakes at Bessy-II [29] and magnetically sensitive measurements at Alba [30]. Despite the potential of TXM spectromicroscopy, the technique is used primarily for tomography and cryo-tomography (at which it excels) as well as magnetic sensitive imaging and magnetic dynamics (at which it excels). Even when the current challenges of uneven illumination, focal and image drift are solved, there will still be issues with the much higher dose that is inevitable in TXM as compared to STXM, since the inefficient zone plate optic is located after the sample rather than before it. There are very nice examples of time-dependent imaging of magnetic dynamics using TXM [31], but even in this area, where the full field aspect of TXM might seem to be far superior to point-mode imaging in STXM, the record time resolution in magnetic dynamics is held by STXM (~10 ps in low-alpha mode at Maxymus, Bessy-II [32]). The ability in STXM to do sub-ps accuracy timing between single photon detection, the bunch-mode trigger and the timing of a magnetization triggering or periodic event, far exceeds the timing accuracy that is possible in TXM due to jitter in camera capture triggering and the relatively slow frame rates.

3.2. Spectromicroscopy in STXMs

As is clear from Fig. 2, there has been tremendous growth in both the number of soft X-ray STXMs and their output over the last 10–15 years. In fact, based on numbers of publications (either in absolute terms or per instrument), STXM is now the most productive of the four common soft X-ray spectromicroscopy techniques. This popularity is related to the broad range of sample systems and processes to which it has been applied. It is particularly powerful for speciation studies of radiation sensitive soft matter samples which are difficult or impossible to study with electron beam based spectromicroscopies such as electron energy loss (EELS) or X-ray fluorescence (EDX) in transmission (TEM) or scanning electron microscopes (SEM). It also has significant advantages for radiation sensitive samples relative to the other 3 types of soft X-ray spectromicroscopies which typically must use much larger doses to get similar quality spectral information due to aspects of the optics (TXM) or intrinsically low yield electron emission processes (SPEM, XPEEM). An interesting comparison in this regard is Fig. 8 which shows the Ti 2p and O 1s NEXAFS spectra of a single $NaTiO_x$ sample, from the same batch as that studied by TXM [28]. Since this study was performed at the CLS beamline 10ID1 for which the source is an elliptically polarizing undulator (EPU), it was possible to do detailed studies of the linear dichroism of the same nanorod by rotating the spatial orientation of the electric vector of the linearly polarized light by adjusting the phase of the EPU [33]. The STXM-generated Ti 2p spectra are in good agreement with the TXM results [28] (Fig. 7). This removed questions raised in the TXM study as to the possibility that the apparent peak shifts were reflecting different chemistry of the two different nanorods, rather than linear dichroism (these types of new materials samples are typically a mixture of a number of different but closely related structures). In addition the spectral resolution of STXM is somewhat higher than the Bessy-II spectro-TXM. In addition to also investigating the O 1s edge, a significant extension of the scope of the investigation has been to use STXM to measure the Ti 2p

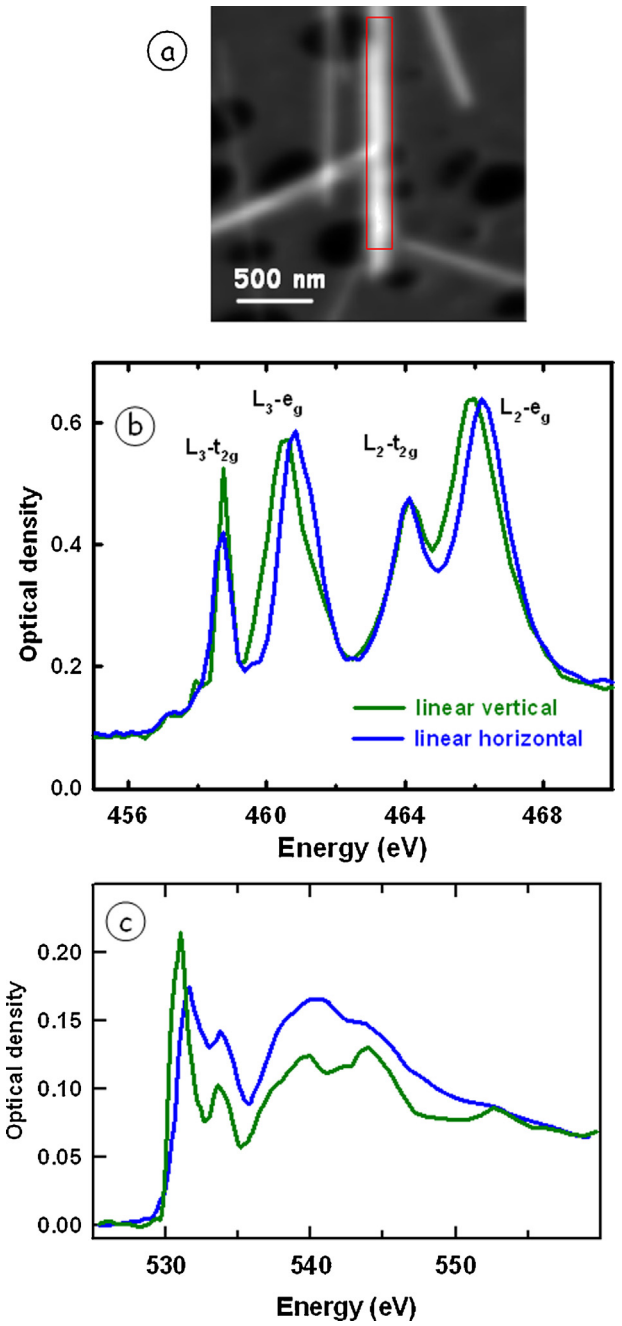

Fig. 8. (a) STXM image at 462 eV of a $NaTiO_x$ nanorod sample. The red rectangle is the region from which the polarization dependent (b) Ti 2p and (c) O 1s spectra of the same nanorod were obtained using image sequence procedures. The orientation of the E-vector relative to this nanorod was modified using the EPU (recorded at CLS ID101).

and O 1s spectra with the E-vector along-rod and across-rod, with the sample mounted at both normal incidence and tilted by 30°. Appropriate trigonometric analysis of these results has provided unique 3D dichroic signals along the 3 principle axes of the nanorods [34]. The results are in reasonable agreement with high level *ab initio* calculations of the dichroic spectra. This combined experimental-theoretical study is providing new insights into both the geometry of the $NaTiO_x$ nanorods and their electronic structure.

As this article is meant to be illustrative rather than comprehensive, I will just mention some of the major areas where STXM spectromicroscopy is being applied with a few key references for each. In my view one of the biggest areas of impact has been in biogeochemistry where STXM is able to give a balanced, quantitative, spatially resolved speciation analysis of the mineral and biological components. In this broad area, there are many STXM studies of soils [35], biomineralization [36], toxic species mobility and immobilization in the environment [37], etc. Many of these studies are done on wet samples, and some provide 3D chemical imaging using spectro-tomography [12]. Most STXM studies detect the transmitted X-rays and thus are sensitive only to majority components (>1% by mass) without any differentiation of location along the path of the X-ray beam through the sample. However total electron yield (TEY) has been developed successfully at many STXM instruments. TEY provides enhanced sensitivity to species at the sample surface [38] since the typical sampling depth in soft X-ray TEY is a few nm. In order to achieve lower detection limits STXMs at Elettra, ALS and CLS have been equipped with soft X-ray fluorescence detectors which enable detection, mapping and spectromicroscopy characterization of minority species at the sub-0.1% level [39,40]. Visible light detection (X-ray excited optical luminescence, XEOL) has also been demonstrated in STXM [41,42], which allows sensitive detection of luminescent species as well as complementary near IR – visible – UV spectroscopy.

3.3. Spectromicroscopy in XPEEMs

Although the PEEM method and commercial instrumentation was developed long ago for lab applications [3] it was only relatively recently [30] that such instruments have been used with synchrotron radiation to enable spectromicroscopy. As UHV surface science instruments, their forte is the chemical analysis and imaging of surfaces with sub-monolayer sensitivity. Most XPEEMs are set up to perform *in situ* deposition of adsorbates on well characterized substrates under controlled temperatures, often ranging from 100–2500 K. Many metal on metal and metal on semiconductor systems have been explored [3]. However XPEEM has a significant sampling depth – in NEXAFS mode it is 4–10 nm, depending on the material – and thus XPEEM is also a useful technique for spectromicroscopy of many types of samples, as long as the near surface region is representative of the bulk. Fig. 9 shows results from an XPEEM study of a $Cr_2O_3(0001)$ thin film sample [43] in which X-ray magnetic circular dichroism (XMCD) [44] at the Cr 2p edge was used to study voltage control of surface magnetization domains. Chromia, Cr_2O_3, is a magneto-electric antiferromagnet in which a very unusual specific surface magnetic order enables electric control of a net surface magnetic moment, which is robust against surface roughness. XPEEM-XMCD probes magnetic states at the surface. Above the Néel temperature the surface has a single magnetic state which is determined by the bulk magnetic properties (Fig. 9a). On cooling to below the Néel temperature, in the absence of magnetic or electric fields, the magnetoelectric effect of Cr_2O_3 gives rise to an electrically induced magnetic moment, which in turn locally selects and stabilizes one of two antiferromagnetic 180° domains, which are seeded by unpaired spins at the surface. Magnetic contrast is seen at 223 K in the multi-domain state after zero-field cooling with a characteristic domain size of 3–5 μm, and a random 50:50 mix of two magnetic states (Fig. 9b). However, with cooling in the simultaneous presence of axial electric and magnetic fields, there is a strong preponderance of one domain (Fig. 9c). The dominant domain is much larger in size than when cooling is performed only in the presence of a magnetic field. The selection of 1 magnetization orientation clearly demonstrates electric control of surface magnetic domains.

Although XPEEM is naturally suited to studies of conducting metallic and semiconductor samples, it has also been applied successfully to organic and insulating samples. If an insulating organic

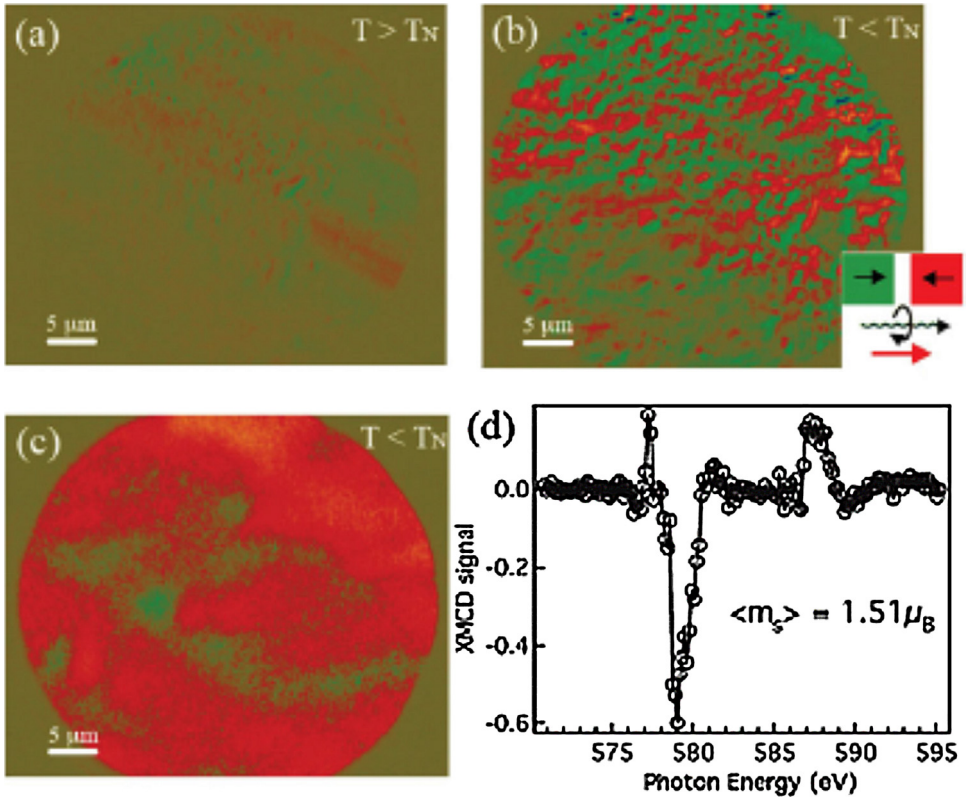

Fig. 9. (a) Cr_2O_3(0001) film imaged by XPEEM using circular polarized light at the Cr 2p edge. (a) Magnetic contrast (XMCD) is not observed at 584 K, above T_N the Néel temperature, (b) a random, multi-domain magnetic surface state is observed after cooling below T_N. The inset indicates the qualitative spin polarization in the image with respect to positively circularly polarized incident light. (c) A nearly single-domain state is observed at 223 K after magnetoelectric field cooling. (d) XMCD spectrum recorded from within one domain (data recorded at CLS-SM XPEEM) (from [43], used with permission, Rights Link license 3572300648352).

film is sufficiently thin (in my experience, below 50 nm), there is sufficient electrical transport to a conductive substrate that the surface field is stable and imaging and spectromicroscopy can be performed. This mode has been used to study polymer thin films [45] as well as protein and peptide interactions with polymeric biomaterials [46]. In situations where the insulating material is too thick it is still possible to successfully perform XPEEM spectromicroscopy if the surface is modified to supply a lateral conducting metal layer with a region thinned to a few nm to enable electron escape from the underlying sample of interest [47]. A very elegant and interesting application of this approach is to biominerals such as carbonate sea urchin teeth and mollusk shells. Fig. 10 presents a number of examples in which XPEEM spectromicroscopy at the Ca 2p edge has been used to identify the spatial distribution of polymorphs of $CaCO_3$ as well as their crystalline orientation [48]. The structures typically are found in the form of very fine 'bricks' of alternating orientation. Fig. 8 of [48] presents similar PIC maps of the shells from 8 different mollusk species, illustrating both common features and variability among species. These types of polarization-dependent imaging contrast (PIC) images, which are due to linear dichroism of anisotropic structures, oriented in different spatial directions, are providing useful insights into biomineralization and the role of thin organic interlayers between the individual domains which appear to guide the growth.

3.4. Spectromicroscopy in SPEMs

The most recently developed and perhaps the most challenging soft X-ray spectromicroscopy is arguably scanning photoemission electron microscopy (SPEM) which combines a dispersive electron spectrometer, a zone plate focusing system and a zone plate or sample scanning system. Despite the challenges a large amount of high quality science on many different surface and materials systems has been generated by synchrotron SPEMs, perhaps because SPEM is closely related to lab-based spatially resolved X-ray photoelectron spectrometers (XPS) and thus there is a large community of users who can take readily appreciate and take advantage of the enhanced spatial resolution and the access to tunable incident light that synchrotron SPEM provides. Angle resolved photoemission (ARPES) is a photoelectron spectroscopy that provides experimental band structures which are very useful to understand novel complex electronic systems such as high-T_c superconductors, magnetic semiconductors, Rashba systems, topological insulators and other exotic materials that arise from complex, highly coupled electronic systems. One of the challenges in this field is the difficulty of making single crystal samples sufficiently large for spectroscopy XPS systems. Thus a SPEM system with versatile sample orientation manipulation capable of ARPES is of great interest to allow studies of sub-micron areas such that ARPES data can be obtained from very small single crystals or single domain appropriately oriented regions in a polycrystalline sample. While the first ARPES results from a submicron area were obtained with a beam focused with Kirkpatrick-Baez optics [49], the first sub-micron ARPES using zone plate optics was reported by Rotenberg et al. [50] using an extension of an existing SPEM at the ALS in a proof-of-principle experiment. New SPEMs optimized for nano-ARPES have recently been built at Soleil (Antares) and at the ALS (Maestro). Fig. 11 presents recent nano-ARPES results from the Antares SPEM in which band structures have been obtained from sub 100 nm regions of graphene on the C-face SiC [51]. These results showed that multilayer graphene on C-face SiC exhibits multiple π bands, indicating

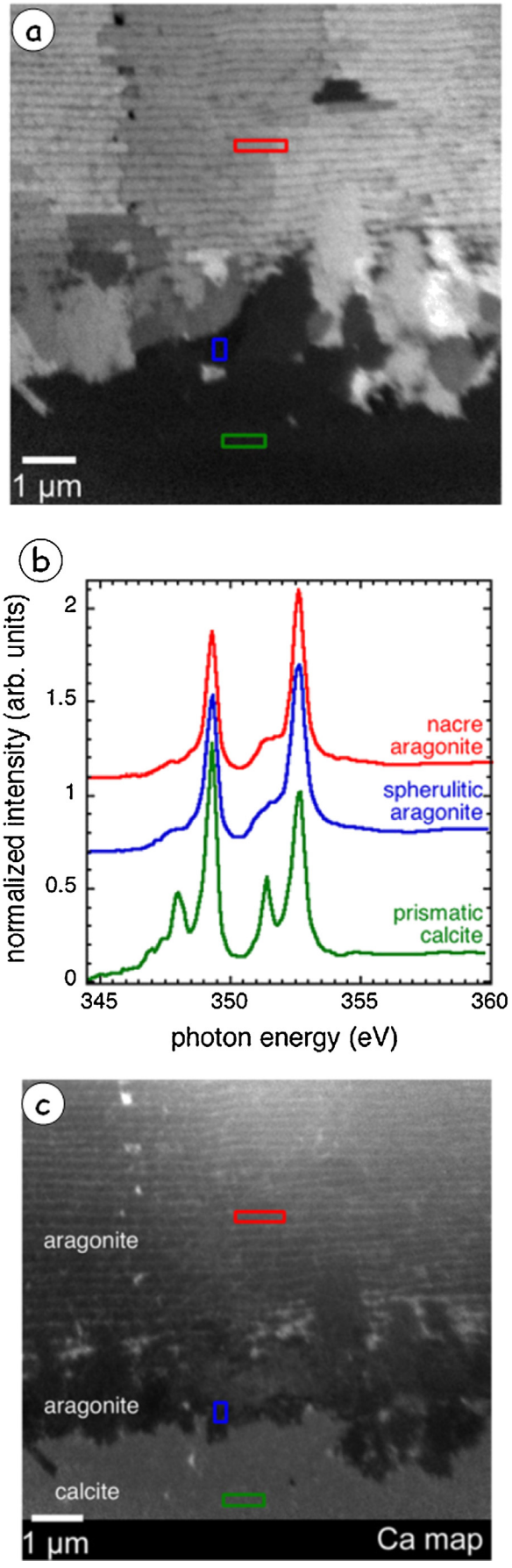

Fig. 10. (a) XPEEM polarization dependent imaging contrast (PIC) map of a red abalone shell. This PIC map is the ratio of images recorded at 290.3 eV (C 1s → π*) and 301.5 eV (C 1s → σ*), with the polarization vector at 45° from the vertical nacre growth direction. (b) Ca 2p spectra and (c) Ca 2p spectromicroscopy (ratio of images at 351.6 eV and 345 eV) identifies the nacre (top) as aragonite and the prismatic layer (bottom) as calcite, with spherulitic aragonite crystals in between. The different gray levels in (a, c) indicate different crystal orientations (from [48], used with permission, Rights Link license 3570551396232).

that the interaction between graphene layers on C-face and Si-face SiC is similar, contrary to other suggestions [52].

4. Ptychography

Ptychography is a coherent diffraction imaging (CDI) technique that uses an X-ray spot created by KirkPatrick-Baez optics or Fresnel ZPs [53] to generate an array of diffraction images from a series of overlapping points on a sample (Fig. 12). The requirement that the solution of the amplitude, phase and illumination components of the reconstruction for each CDI must match in the 6 adjacent CDI images provides a powerful constraint which leads to rapid and reliable convergence of the analysis compared to all other CDI methods. Spatial resolutions of 10 nm in the hard X-ray [54] and below 3 nm in the soft X-ray [55] have been achieved. Ptycho-tomography has also been implemented with angle scanning of samples to produce quantitative 3D density maps with a 3D isotropic spatial resolution of 16 nm [56]. At present hard X-ray ptychography and ptycho-tomography is well established, with instrumentation accessible to general users through peer review access at a number of facilities, including SLS and PETRA-III. Ptychography in the soft X-ray region is less well developed, largely because cameras for direct sensing X-rays have a smaller dynamic range and are less efficient than hard X-ray area detectors. The COSMIC beamline at the ALS will be the first beamline dedicated to soft X-ray ptychography. It is expected to be completed by end of 2015, and to be open to general users 1 or 2 cycles after that. Exploratory and developmental soft X-ray ptychography and ptycho-tomography is being carried on other beamlines at the ALS (5.3.2.1, 11.0.2) [55,57], as well as at the CLS (10ID1).

Fig. 13 presents recent results on spectro-ptychography of $LiFePO_4$ materials, used in lithium ion batteries [55,58] from the Nanosurveyor instrument which is a STXM-like instrument at the ALS dedicated to ptychography. Just as with regular STXM, X-ray absorption spectra can be obtained from ptychography by recording data at multiple photon energies and extracting the amplitude (and phase) signal from the same region of space. Fig. 13a are amplitude and phase spectra for the fully lithiated ($LiFePO_4$) and fully delithiated ($FePO_4$) materials. There is a clear shift in the absorption peak of the Fe $L_3 \rightarrow 3d$ transition from the Fe(II) to the Fe(III) species. While the changes are more subtle, there are also changes in the phase signal. Both signals can and have been used in the chemical mapping. Fig. 13b is the bright field STXM image. The spatial resolution and clarity of detail in the amplitude (Fig. 13c) and phase(Fig. 13d) images is much better, in part due to improved resolution and in part due to alternative contrast mechanisms, especially in the phase channel. Fig. 13e is a color coded composite of the component maps for $LiFePO_4$ (Fe(II), red) and $FePO_4$ (Fe(III), blue) derived by a full treatment of the ptychography data measured at 31 energies (see reference spectra in Fig. 13a) using an automated procedure of complex-valued principal component analysis followed by expectation–maximization clustering (k-means algorithm), and finally singular value decomposition, using both phase and amplitude signals [55]. What is fascinating about this example, beyond the impressive technical achievements and improved spatial resolution, is that other studies [58] have shown that the lithiation and delithiation processes occur sequentially, with all of a particle transforming at once. Thus it is rather rare to find a crystal in mid-transformation, yet this is

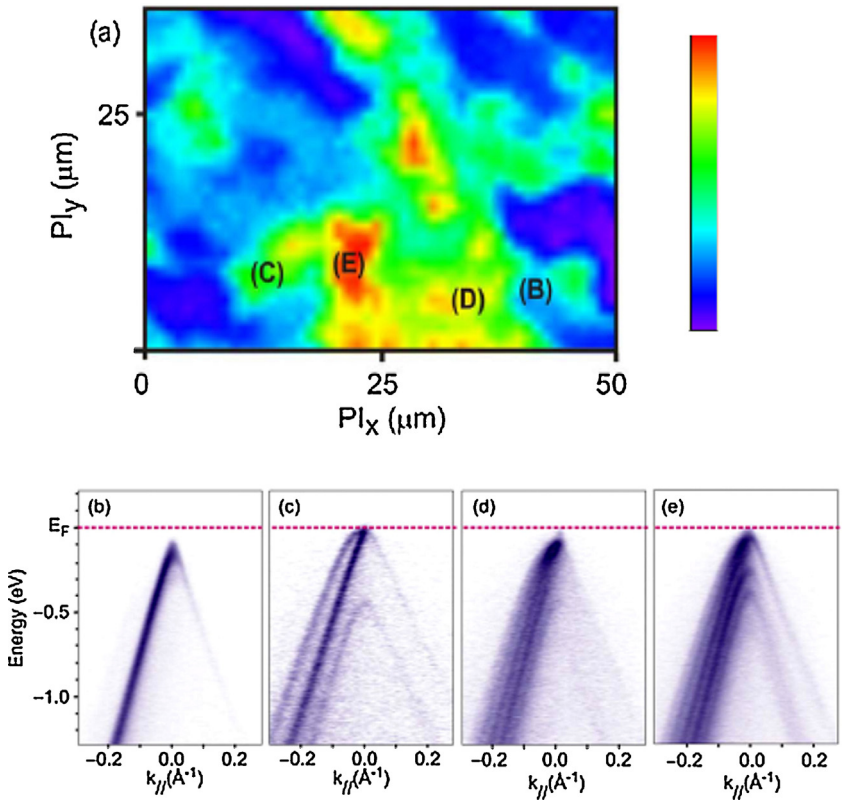

Fig. 11. (a) SPEM image of graphene on C-face SiC(000-1) formed from the p-band intensity integrated from 0 to 0.5 eV below E_F, recorded using $h\nu = 100$ eV with a spatial resolution of 120 nm. (b)–(e) Nano-ARPES band maps recorded, at $\phi = 59^\circ$ along the Γ-K-M direction from 4 different graphene grains at the labeled positions in (a) (adapted from [50], open access).

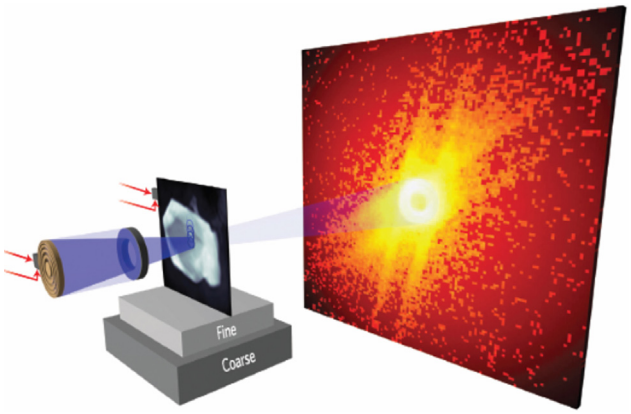

Fig. 12. Schematic of ptychography. A zone plate focused 60 nm spot of coherent soft X-rays is scanned over a sample in 40 nm increments to ensure overlap of the probed areas. Diffraction data are recorded by a direct X-ray sensitive camera downstream of the sample. The sample position is stabilized with respect to the zone plate by an interferometer (red arrows) that measures relative displacements in the scanning directions with 1.5 nm resolution. After appropriate analysis, the distribution of photons scattered outside the central annulus (the expanded zone plate illumination) provide the increased spatial resolution of ptychography relative to the corresponding bright field STXM image (from [53], used with permission, Rights Link license 3570550525651).

the type of data that is needed to give insights into how to further optimize lithium battery materials to achieve a more stable solid electrolyte interphase (SEI) and thus a higher performance system. In this case, the presence of the cracks along the C-axis are likely a manifestation of the expansion and contraction stresses in the lithiation/delithiation processes.

A second example of spectro-ptychography is presented in Fig. 14, where it was used to determine the Fe L_3 spectra and associated X-ray magnetic circular dichroism (XMCD) of individual magnetosomes in a cell of *Magnetovibrio blakemorei* strain MV-1 magnetotactic bacteria (MTB). For a number of years we have been using STXM-XMCD to study various aspects of the magnetism of MV-1 and other MTB species [59–61]. Fig. 14a is a STXM image of several cells. The cell on the left with the horizontal magnetosome chain was selected for the ptychography study, since only horizontal chains on samples tilted out of plane give rise to XMCD signal [59]. The 30° sample tilt means that the cells and magnetosomes are foreshortened horizontally by ∼14%. Fig. 14b is the amplitude image at 708 eV, where the XMCD is strongest, derived from ptychography patterns measured using circularly polarized light (95%). The spatial resolution in the ptycho amplitude image is estimated from edge sharpness to be ∼7 nm, which is much better than the ∼30 nm spatial resolution of bright field STXM images of in-cell MV1 magnetosomes, using the standard 25 nm outer zone, zone plates [60]. Fig. 14**c** is a color coded composite of the parallel and antiparallel XMCD signals from this chain, derived from ptychography amplitude images at 708.2 eV measured with left and right circular polarized X-rays. One of the themes of a previous study has been the presence of a significant sub-population in MTB where individual cells contain magnetosome chains with what appear to be gaps (missing magnetosomes), and in a further sub-set of such cells the magnetization of the sub-chains on opposite sides of the gap are opposite [61]. This is exactly the case in this cell, now seen with significantly higher spatial resolution than any prior study due to use of ptychography. In addition to higher spatial resolution imaging, ptychography provides much stronger spectral signals of small objects such as magnetosomes, not just because of its higher spatial resolution, but also because the ptychographic reconstruction derives, and corrects for the shape and propagation of the X-ray wave front. This point is made clearly in Fig. 14d which compares the strength of the Fe L_3 spectrum of magnetosomes

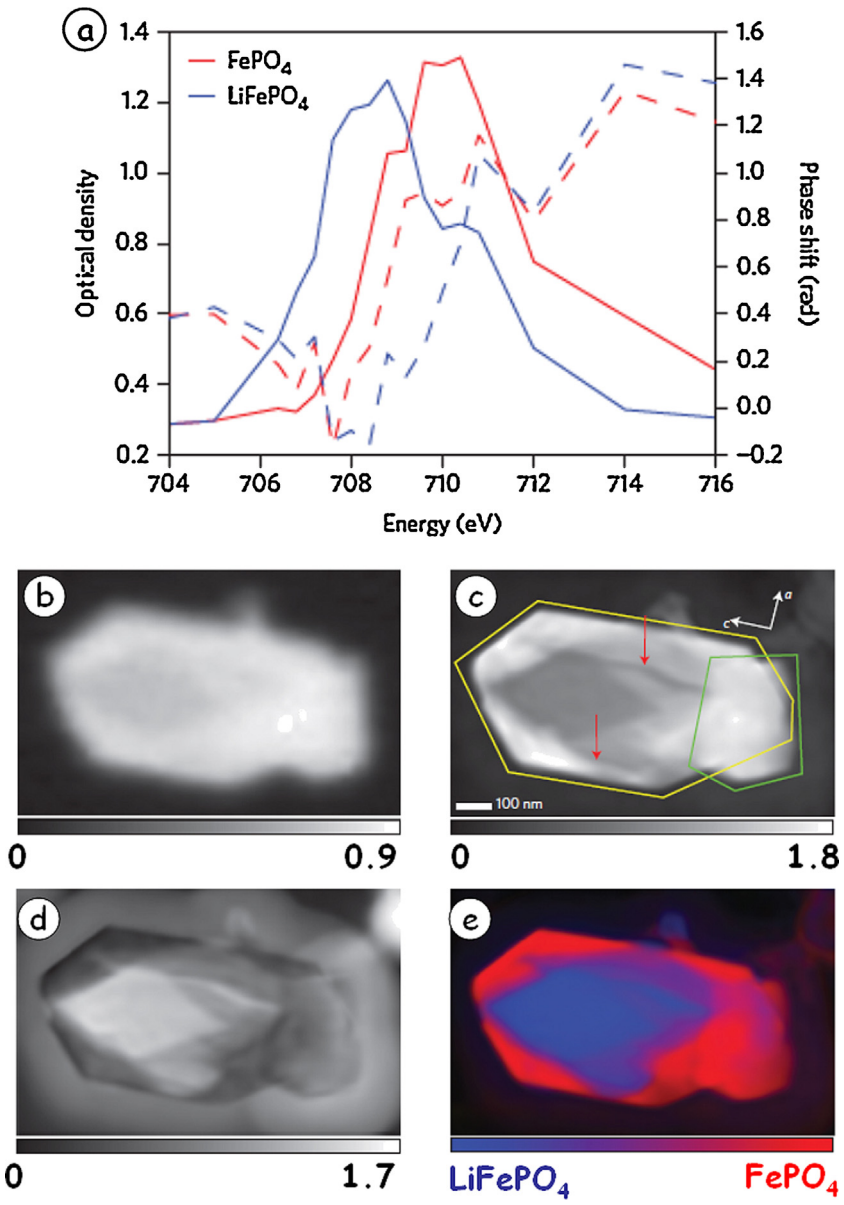

Fig. 13. (a) X-ray absorption and phase spectra of $FePO_4$ and $LiFePO_4$ measured in STXM. (b) Optical density map at 710 eV of a partially delithiated grain of $LiFePO_4$ measured with a ZP having a 60 nm outer zone width (diffraction limited resolution of 72 nm), (b) Optical density map derived from analysis of the ptychography data recorded simultaneously (pixel size, 4.0 nm. scale bar, 100 nm). Multiple particles, which could only be detected by ptychography, are outlined (yellow), along with cracks along the crystallographic c axis (red arrows). The a and c crystallographic axes are indicated by white arrows; the b axis is parallel to the incident X-rays. (c) Phase of the ptychographic reconstruction at 709.2 eV, showing maximum relative phase shift between the end members. The halo around the particle is carbon contamination, which builds up with X-ray exposure and is not apparent in the absorption images. (d) Colorized composition map calculated from the full complex refractive index (from [55], used with permission, Rights Link license 3570550525651). (data recorded at ALS 11.0.2 and 5.3.2.1).

measured by ptychography with those measured by conventional STXM using 25 nm and 60 nm outer zone plates. This is a general observation which points to significant benefits from ptychography in terms of spectroscopic and thus chemical sensitivity, in addition to the well documented enhancements of improved spatial resolution.

5. Perspective for near future developments

5.1. Instrumentation

Several trends currently in play are going to make significant improvements in soft X-ray spectromicroscopy and ptychography in the near future. Diffraction limited storage rings such as NSLS II, Max IV and Sirius will provide at least an order of magnitude improvement in brightness and coherence in the soft X-ray region (and even more dramatic increases in the hard X-ray region) [62–64] which will provide large improvements in the performance of zone plate optics and coherent diffraction signals. With these new sources the point probe techniques – STXM, SPEM and ptychography – will have significantly improved performance and throughput. SPEM in particular should greatly benefit from improved brightness which will increase the photon density of the focused beam, giving more photoelectron signal. Given the 5- to 10-fold improvement that ptychography provides relative to the focused spot size [53], combined with the increasing brightness of newer 3rd generation and diffraction limited light sources, it is likely that most of the existing STXMs and all new STXMs will

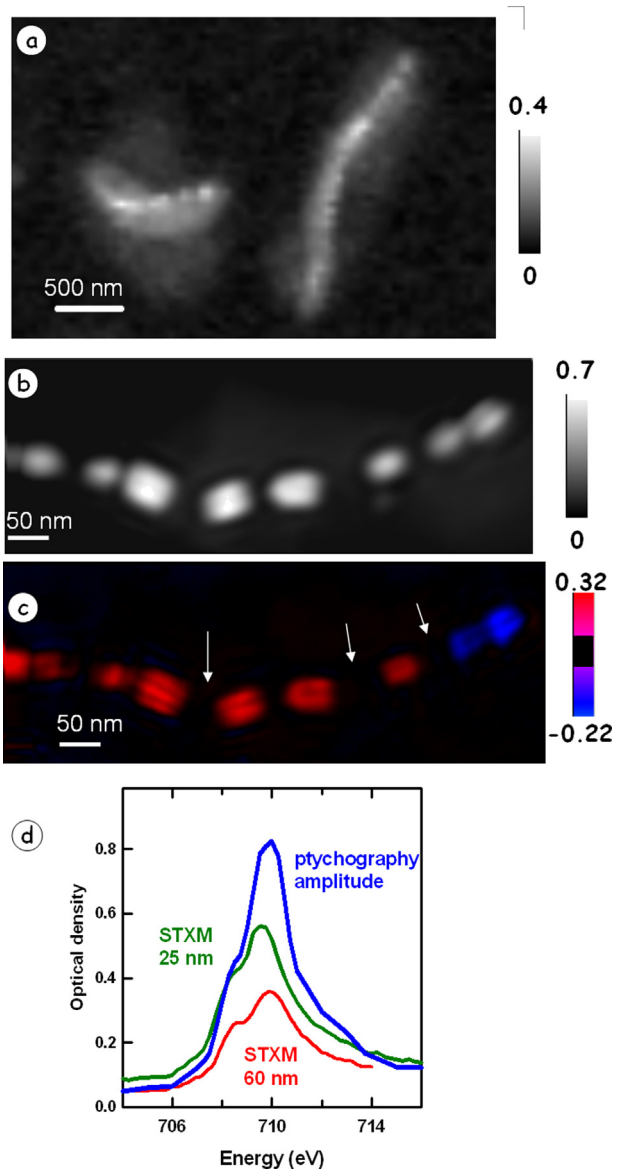

Fig. 14. (a) STXM image (60 nm zone plate) of several cells of *Magnetovibrio blakemorei* strain MV-1 magnetotactic bacterium, measured at 710 eV. The ptychography measurements were made on the intact cell on the left. (b) Optical density image of the magnetosomes in the cell derived from ptychography data (20×8 diffraction patterns, $560 \times 220\ nm^2$, 300 ms/image) measured at 708.2 eV (the energy of peak magnetic contrast). (c) Magnetic map at 708.2 eV of the magnetosomes in this cell from single energy X-ray magnetic circular dichroism (XMCD)—the difference of ptychography OD images measured at 708.2 eV with the photon spin parallel and anti-parallel to the magnetic moment. There are gaps in the chain (white arrows) and the orientation of the magnetic vector is opposite on each side of the right most gap. The uneven distribution of intensity within individual magnetosomes is an artifact of the ptychographic data processing. (d) Comparison of Fe L_3 spectra of MV-1 magnetosomes recorded with STXM using 25 nm and 60 nm outer-zone width zone plates, and with ptychography (60 nm ZP, 50 nm pixel spacing). In each case left circular polarized light was used (data recorded at ALS 11.0.2).

be equipped with appropriate high dynamic range cameras, high performance computing, and other instrumentation to enable ptychography as a routine, high resolution extension of conventional STXM imaging.

Since ptychography, especially spectro-ptychography and tomo-ptycography, generates very large data sets (0.2 Gb/image, multi-Tb/day [65]) improvements in the storage, archiving and processing of large data sets are needed, as well as faster computational and display systems. Fortunately with the decreasing cost of both storage and computing, the rapid expansion of the use of graphical processors (GPU) for scientific computing, and the development of reliable, powerful and fast ptychography reconstruction algorithms, these issues are being taken care of and are unlikely to be significant barriers to rapid implementation of soft X-ray ptychography. Even now, the SHARP routine [65] is fast enough that data reduction is possible in about the same time as acquisition so that images can be inspected a few minutes after being recorded. There will be some very fascinating developments in applications of ptychography. On the one hand almost all samples studied to date by soft X-ray ptychography have morphologies and densities that lead to strong coherent X-ray scattering. Thus there is some question if there will be significant signal from the weaker, less structured components (polymers, biological macromolecules etc) which tend to be important samples for the conventional STXM community (compare Fig. 14a and b). On the other hand, the improved spatial resolution, new signal channels (phase, illumination) and novel approaches to data analysis [55] offer opportunities for qualitatively new information. Better cameras, either direct detection soft X-ray systems or scintillator/visible light systems, are needed to fully take advantage of soft X-ray spectro-ptychography. While direct detection soft X-ray cameras exist they typically have limited dynamic range and slow data transfer rates. For example, with the camera used to record the data of Fig. 14, the duty cycle was less than 10% due to the long time it takes to transfer each image from the camera. Recently a consortium of the US Department of Energy laboratories have produced a direct soft X-ray camera with good dynamic range and very high image transfer rates which is now used on some ptychography measurements at the ALS. A soft X-ray imaging system with the performance of the Dectris (www.dectris.com) cameras for hard X-rays would be ideal. In some ways a scintillator/visible light system [66] would also be a good solution since this would reduce the risk of damage to a direct X-ray camera if it is exposed to the focused X-ray probe. It would also allow use of the very high performance, single photon sensitive visible light cameras that are now available for optical super-resolution microscopy [67]. However at present the efficiency of the scintillators is a limiting factor.

In the area of electron detection based soft X-ray microscopes, there has been a large effort for more than a decade to implement aberration corrected optics in synchrotron based XPEEM systems. There are commercially available optics, as well as custom systems implemented at Bessy-II [68] and the ALS [69]. While these systems do provide significantly improved spatial resolution for mono-energetic electron distributions, as in LEEM, there has been only limited resolution gains in XPEEM mode, i.e. when synchrotron light is used. The corrected optics provide improved electron transmission [69] which is very helpful when studying radiation sensitive samples. Further improvements in the aberration correctors and their implementation in XPEEM mode are needed. A novel type of PEEM is trPEEM [67] where imaging time of flight electron detection is used, taking advantage of pulsed light sources such as lasers and synchrotrons for spectral imaging with simultaneous spatial and temporal resolution. Continual advances in electronics and narrow pulse light sources (e.g. free electron lasers, FELs) offer interesting opportunities for this method. In SPEM, advanced electron analyzers, improved motion stages and extensive interferometer control are making possible systems that not only can do XPS and NEXAFS spectral imaging, but also fully momentum resolved ARPES systems with sub-100 nm spatial resolution [70]. Recently a SPEM has been developed at the ALS which differentially pumps the electron analyzer enabling ambient pressure (up to 10 torr) photoemission with sub-100 nm spatial resolution [52]. Higher brightness light sources will significantly benefit ambient-SPEM, although there are significant challenges with respect to sample contamination which need to be overcome.

With respect to spectromicroscopy, full field spectro-TXM is perhaps the least developed of the 4 common soft X-ray microscopes. The pioneering work at Bessy-II [17] demonstrating that spectro-TXM can indeed be made to work with a fully monochromated beam points the way. This type of system could greatly benefit from adopting the approaches now common in STXM and SPEM to use active interferometer control of the relative positions of the ZP, sample and objective lens. This would allow for automated, precise tracking of focus and lateral position on the sample as photon energy is changed, which at present seems to be a limitation of spectro-TXM as compared to STXM. Among the 4 techniques it would seem TXM has least to benefit from the upcoming higher brightness light sources.

Fig. 2 indicates that, at present, STXM is the most productive of the soft X-ray microscopes. Indeed at most light sources with operating STXMs, the STXM beamline is typically the most competitive across the whole facility in terms of peer reviewed access. While there are more STXM facilities coming (see Table 1), it should be possible to increase the efficiency of existing STXMs by introducing faster motion stages. At present, even with very light sample stages, the fastest line scan rate is perhaps 10 Hz. A system constructed entirely from piezo stages has recently been developed at Photon Factory [71], and that system should be able to work at very fast scan rates. Atomic force microscopes (AFM) have similar issues with respect to tip scanning, and there are now commercial systems able to scan at 100 Hz, enabling video-rate imaging [72]. Similar approaches, particularly those involving scanning the ZP lens rather than the sample, should be possible in STXM. At present, undulator based soft X-ray STXMs routinely use aperturing, not for energy resolution or to achieve diffraction limited focusing, but to reduce the incident flux to within the linear range of the detector (typically 20 MHz). With improved detectors and faster scanning the full potential of these systems could be realized.

For each of these techniques an important and ongoing development is to combine them with other analytical and imaging methods to achieve a synergistic correlative method. A nice example of this is the combination at the XM-2 (NCXT) facility of a TXM microscope optimized for automated X-ray cryo-tomography with a system for optical cryo-tomography with transmission or UV–vis fluorescence detection [73]. One can imagine combining a commercial optical super-resolution microscope with STXM or TXM. In many cases correlative microscopy is achieved in separate instruments with appropriate sample holders and fiducialization systems used to facilitate study of the same sample area/volume by a number of different techniques. Further instrument improvements in these areas offer simple and effective means to increase the impact of soft X-ray spectromicroscopy.

5.2. Applications

Any advanced analytical imaging system is only of value if it can be applied to problems of significant fundamental and/or technological importance. Each of the 4 common soft X-ray spectromicroscopies have demonstrated areas where they are 'the best tool for the job'. TXM excels at cryo-tomography of biological samples, particularly whole cells, and at magnetic imaging and dynamics [31]. SPEM provides the power and clarity of XPS for surface analysis. XPEEM is finding many useful applications in the area of thin film and surface analysis, as well as biomaterials [46] and biomineralization [47]. STXM is perhaps the most versatile of the four methods since it has been used to study a very wide range of sample types and processes, including picosecond magnetization dynamics [32].

Studies of energy materials and processes are an area of rapid development and high scientific activity at many light sources. While investigative and post-mortem analysis is the most common approach, increasingly soft X-ray spectromicroscopes are being used for *in situ* and even *operando* studies, whereby the sample is conditioned or transformed inside the microscope, using processes similar to those in a real world application. Thus STXM has been applied to *in situ* spectro-electrochemistry [74–76], *in situ* controlled humidity studies [77–79], *in situ* catalysis [80], etc. SPEM has been applied to *in situ* studies of polymer electrolyte membrane fuel cells [81] and *operando* studies of solid oxide fuel cell systems [82]. XPEEM is often used for *in situ* thin film growth studies, as well as variable temperature investigations [43]. With the recent development of single atomic layer graphene wet cells [83], it will be possible to apply electron detection based spectromicroscopies to samples and processes in a liquid environment. A wider range of applications of *in situ* methods will be a significant trend in soft X-ray spectromicroscopy in the coming decade. At the same time, *in situ* and *operando* capabilities in other types of analytical microscopies are advancing very rapidly so it is important to be aware of those developments and to choose projects where the strengths of soft X-ray spectromicroscopy can be put to good use. In particular, systems to allow heating, fluid flow, electrochemistry, gas-surface reaction, etc, are now commercially available for use in (S)TEM. I expect the spatial resolution of aberration corrected S(TEM), currently sub 100 pm, will be better than anything achievable in soft X-ray spectromicroscopy for the foreseeable future (*ok, you smart instrumentation folks, prove me wrong!*). Thus it will be in the areas of detailed spectroscopy and applications to highly radiation sensitive samples where soft X-ray spectromicroscopy will have significant advantages. Scientific problems requiring these capabilities are the areas where *in situ* and/or *operando* soft X-ray spectromicroscopy has its greatest potential for impact.

All microscopy techniques continually strive for higher spatial resolution. It seems that soft X-ray ptychography will enable routine studies with sub-10 nm spatial resolution, a scale which many define as that of true nano-science. Extending soft X-ray ptychography so as to fully exploit its new spectral content and to enable cryo- spectro-ptychography and cryo-tomo-spectro-ptychography will be challenging areas with much potential reward in the coming years. It is now rather trite to say this, but it is appropriate, in the context of continual improvements in light source stability and brightness, to end this perspective by saying, '*the future for soft X-ray spectromicroscopy is bright indeed!*'.

Acknowledgments

I thank colleagues, group members and collaborators who provided material for this article. Ptychography measurements were performed at ALS BL 11.0.2. STXM measurements were performed at BL 11.0.2 and 5.3.2.2 at the Advanced Light Source, which is supported by the Director, Office of Energy Research, Office of Basic Energy Sciences, Materials Sciences Division of the U.S. Department of Energy, under Contract No. DE-AC02-05CH11231, and at the Canadian Light Source spectromicroscopy facility (BL 10ID1), which is supported by the Canadian Foundation for Innovation, Natural Sciences and Engineering Research Council of Canada, the University of Saskatchewan, the Government of Saskatchewan, Western Economic Diversification Canada, the National Research Council Canada, and the Canadian Institutes of Health Research. I especially thank the expert support of the staff scientists at the ALS – Tolek Tyliszczak, David Kilcoyne and David Shapiro – and at the CLS—Jian Wang, Chithra Karunakaran and Jay Dynes.

Appendix A. Supplementary data

Supplementary data associated with this article can be found, in the online version, at http://dx.doi.org/10.1016/j.elspec.2015.05.013

References

[1] A.P. Hitchcock, Soft x-ray imaging and spectromicroscopy, in: Gustaaf Van Tendeloo, Dirk Van Dyck, J. Stephen, Pennycook (Eds.), The Handbook on Nanoscopy, II, Wiley, 2012, pp. 745–791 (Chapter 22).

[2] H. Ade, A.P. Hitchcock, NEXAFS microscopy and resonant scattering: composition and orientation probed in real and reciprocal space, Polymer 49 (2008) 643–675.

[3] E. Bauer, Surface Microscopy with Low Energy Electrons, Springer, NY, 2014.

[4] S. Günther, B. Kaulich, L. Gregoratti, M. Kiskinova, Photoelectron microscopy and applications in surface and material science, Prog. Surf. Sci. 70 (2002) 187–260.

[5] M. Howells, C. Jacobsen, T. Warwick, in: W. Peter, Hawkes, C.H. John, Spence (Eds.), Principles and Applications of Zone Plate X-Ray Microscopes in Science of Microscopy, Springer, NY, 2007.

[6] B. Kaulich, P. Thibault, A. Gianoncelli, M. Kiskinova, Transmission and emission x-ray microscopy: operation modes, contrast mechanisms and applications, J. Phys.: Condens. Matter 23 (2011) 083002.

[7] R. Falcone, Ch. Jacobsen, J. Kirz, S. Marchesini, D. Shapiro, J. Spence, New directions in x-ray microscopy, Contemp. Phys. 52 (2011) 293.

[8] D. Attwood, Soft X-rays And Extreme Ultraviolet Radiation, Principles and Applications, Cambridge University Press, Cambridge, UK, 2000.

[9] J. Kirz, C. Jacobsen, M. Howells, Soft x-ray microscopes and their biological applications, Q. Rev. Biophys. 28 (1995) 33–130.

[10] J. Kirz, C. Jacobsen, The history and future of x-ray microscopy, J. Phys.: Conf. Ser. 186 (2009) 012001.

[11] J.H. Carpenter, A. Hunt, H. Ade, Resonant soft X-ray scattering: a unique tool for characterizing morphology in organic systems, J. Electron Spectrosc. Relat. Phenom. 200 (2015) (xxxx—this volume).

[12] G. Schmid, M. Obst, J. Wu, A.P. Hitchcock, 3D chemical imaging of nanoscale biological, environmental and synthetic materials by soft X-ray spectrotomography, book chapter in: Characterization Tools for Nanoscience & Nanotechnology, 5 (2015) (in press).

[13] M. Holt, R. Harder, R. Winarski, R. Volker, Nanoscale hard x-ray microscopy methods for materials studies, Annu. Rev. Mater. Res. 43 (2013) 183.

[14] E. Maire, P.J. Withers, Quantitative x-ray tomography, Int. Mater. Rev. 59 (2014) 1–43.

[15] G. Schmahl, D. Rudolph, Lichstarke Zoneplatten als abbildende Sytee für weiche Röntgenstrahlung (High power zone plates a image forming systems for soft X-rays), Optik 29 (1969) 577–585.

[16] G. Schmahl, D. Rudolph, P. Guttmann, O. Christ, Zone-plate X-ray microscopy, Q. Rev. Biophys. 13 (1980) 297–315.

[17] P. Guttmann, S. Rehbein, S. Werner, K. Henzler, B. Tarek, G. Schneider, Nanoscale spectroscopy and tomography with the HZB X-ray microscope: applications in materials and life sciences, J. Phys. Conf. Ser. 463 (2013) 012032.

[18] E. Pereiro, J. Nicolas, S. Ferrer, M.R. Howells, A soft X-ray beamline for transmission X-ray microscopy at ALBA, J. Synchrotron Radiat. 16 (2009) 505–512.

[19] A.L. Pearson, W. Chao, G. Denbeaux, T. Eimueller, P. Fischer, L.E. Johnson, M. Koehler, C.M. Larabell, A. LeGros, D. Yager, D.T. Attwood, Soft x-ray and EUV imaging systems, Proc. SPIE 4146 (2000) 54.

[20] D.Y. Parkinson, G. McDermott, L.D. Etkin, M.A. Le Gros, C.A. Larabell, Quantitative 3-D imaging of eukaryotic cells using soft X-ray tomography, J. Struct. Biol. 16 (2008) 380–386.

[21] P. Guttmann, X. Zeng, M. Feser, S. Heim, W. Yun, G. Schneider, Ellipsoidal capillary as condenser for the BESSY full-field x-ray microscope, J. Phys.: Conf. Ser. 186 (2009) 012064–12073.

[22] H. Rarback, J. Kenney, J. Kirz, X.S. Xie, Scanning x-ray microscopy—first tests with synchrotron radiation, in: E.A. Ash (Ed.), Scanned Image Microscopy, Academic Press, London, 1980, p. 449.

[23] H. Ade, X. Zhang, S. Cameron, C. Costello, J. Kirz, S. Williams, Chemical contrast in x-ray microscopy and spatially resolved xanes spectroscopy of organic specimens, Science 258 (1992) 972.

[24] K.V. Kaznatcheev, C. Karunakaran, U.D. Lanke, S.G. Urquhart, M. Obst, A.P. Hitchcock, Soft X-ray spectromicroscopy beamline at the CLS: commissioning results, Nucl. Instrum. Methods Phys. Res. A 582 (2007) 96–99.

[25] H. Ade, J. Kirz, S. Hulbert, E. Johnson, E. Anderson, D. Kern, Images of a microelectronic device with the X1-SPEM, a first generation scanning photoemission microscope at the National Synchrotron Light Source, J. Vac. Sci. Technol. A 9 (1991) 1902.

[26] B.P. Tonner, G.R. Harp, Photoelectron microscopy with synchrotron radiation, Rev. Sci. Instrum. 59 (1988) 853.

[27] J. Avila, M.C. Asensio, First nanoarpes user facility available at SOLEIL: An innovative and powerful tool for studying advanced materials synchrotron radiation news, 27 (2014) 24.

[28] P. Guttmann, C. Bittencourt, S. Rehbein, P. Umek, X.X. Ke, G. Van Tendeloo, C.P. Ewels, G. Schneider, Nanoscale spectroscopy with polarized X-rays by NEXAFS-TXM, Nat. Photonics 6 (2012) 25–29.

[29] C. Bittencourt, A.P. Hitchcock, X. Ke, G. Van Tendeloo, C.P. Ewels, P. Guttmann, X-ray absorption spectromicroscopy of a thin graphite flake: Imaging and electronic structure via the carbon K-edge, Beilstein J. Nanotechnol. 3 (2012) 345–350.

[30] A. Sorrentino, C. Blanco, C. Quirós, R. Valcarcel, J. Avila, E. Pereiro, S. Ferrer, Magnetic transmission soft x-ray microscopy at mistral (abstract 1P26, Oct), in: Proceedings of 12th International Conference On X-ray Microscopy, Melbourne, AU, 2014.

[31] P. Fischer, Frontiers in imaging magnetism with polarized x-rays, Front. Phys. 2 (2014) 82.

[32] D. Nolle, M. Weigand, P. Audehm, E. Goering, U. Wiesemann, C. Wolter, E. Nolle, G. Schütz, Unique characterization possibilities in the ultra high vacuum scanning transmission x-ray microscope (UHV-STXM) MAXYMUS using a rotatable permanent magnetic field up to 0.22 T, Rev. Sci. Instrum. 83 (2012) 046112.

[33] A.T. Young, E. Arenholz, S. Marks, R. Schlueter, C. Steier, H.A. Padmore, A.P. Hitchcock, D.G. Castner, Variable linear polarization from an x-ray undulator, J. Synchrotron Radiat. 9 (2002) 270–274.

[34] X. Zhu, A.P. Hitchcock, C. Bittencourt, P. Umek, P. Krüger, Individual titanate nanostructures studied by 3d-resolved polarization dependent x-ray absorption spectra measured with STXM, ACS Nano (submitted).

[35] J. Lehmann, D. Solomon, J. Kinyangi, L. Dathe, S. Wirick, C. Jacobsen, Spatial complexity of soil organic matter forms at nanometere scales, Nat. Geosci. 1 (2008) 238–242.

[36] J. Cosmidis, K. Benzerara, Soft x-ray scanning transmission spectromicroscopy, in: E. DiMasi, L.B. Gower (Eds.), Biomineralization Sourcebook, CRC Press, London, UK, 2014.

[37] J.R. Lawrence, G.D.W. Swerhone, J.J. Dynes, D.R. Korber, A.P. Hitchcock, Soft x-ray spectromicroscopy for speciation, quantitation and nano-eco-toxicology of nanomaterials, J. Microsc. (2014), http://dx.doi.org/10.1111/jmi.12156

[38] D. Nolle, M. Wiegand, G. Schütz, E. Goering, High contrast magnetic and non-magnetic sample current microscopy for bulk and transparent samples using soft X-rays, Microsc. Microanal. 17 (2011) 834–842.

[39] A. Alberti, T. Klatka, A. Longoni, D. Bacescu, A. Marcello, A. De Marco, A. Gianoncelli, A. Kaulich, Development of a low-energy x-ray fluorescence system with sub-micrometer spatial resolution, X-ray Spectrom. 38 (2009) 205–210.

[40] A.P. Hitchcock, M. Obst, J. Wang, Y.S. Lu, T. Tyliszczak, Advances in the detection of As in environmental samples using low energy X-ray fluorescence in a scanning transmission X-ray microscope: arsenic immobilization by an Fe(II)-oxidizing freshwater bacteria, Environ. Sci. Technol. 46 (2012) 2821.

[41] C. Jacobsen, S. Lindaas, S. Williams, X. Zhang, Scanning luminescence x-ray microscopy: imaging fluorescence dyes at suboptical resolution, J. Microsc. 172 (1993) 121.

[42] Z. Wang, J. Wang, T.K. Sham, S. Yang, Origin of the luminescence from ZnO/CdS core/shell nanowire arrays, Nanoscale 6 (2014) 9783.

[43] N. Wu, X. He, A.L. Wysocki, U. Lanke, T. Komesu, K.D. Belashchenko, Ch. Binek, P.A. Dowben, Imaging and control of surface magnetization domains in a magnetoelectric antiferromagnet, Phys. Rev. Lett. 106 (2011) 087202.

[44] J. Stöhr, Exploring the microscopic origin of magnetic anisotropies with X-ray magnetic circular dichroism (XMCD) spectroscopy, J. Magn. Magn. Mater. 200 (1999) 470.

[45] S. Minko, M. Müller, D. Usov, A. Scholl, C. Froeck, M. Stamm, Lateral versus perpendicular segregation in mixed polymer brushes, Phys. Rev. Lett. 88 (2002) 035502.

[46] B.O. Leung, J.L. Brash, A.P. Hitchcock, Characterization of biomaterials by soft X-ray spectromicroscopy, Materials 3 (2010) 3911–3938.

[47] P. Gilbert, Photoemission spectromicroscopy for the biomineralogist, in: E. Gower, DiMasi (Eds.), Biomineralization Sourcebook, Characterization of Biominerals and Biomimetic Materials, CRC Press, Boca Raton, FL, 2014, pp. 135–151.

[48] P. Gilbert, Polarization-dependent Imaging Contr ast (PIC) mapping reveals nanocrystal orientation patterns in carbonate biominerals, J. Electron Spectrosc. Relat. Phenom. 185 (2012) 395–405.

[49] P. Dudin, P. Lacovig, C. Fava, E. Nicolini, A. Bianco, G. Cautero, A. Barinov, Angle-resolved photoemission spectroscopy and imaging with a submicrometre probe at the SPECTROMICROSCOPY-3.2L beamline of Elettra, J. Synchrotron Radiat. 17 (2010) 445–450.

[50] A. Bostwick, E. Rotenberg, J. Avila, M.C. Asensio, Zooming in on electronic structure: NanoARPES at SOLEIL and ALS, Synchrotron Radiat. News 25 (2012) 19–25.

[51] L. I. Johansson, R. Armiento1, J. Avila, C. Xia, S. Lorcy, I.A. Abrikosov1, M.C. Asensio, C. Virojanadara, Multiple p-bands and Bernal stacking of multilayer graphene on C-face SiC, revealed by nano-Angle Resolved Photoemission Nature Scientific Reports 4 (2014) 4157.

[52] J. Hass, R. Feng, J.E. Millán-Otoya, X. Li, M. Sprinkle, P.N. First, W.A. de Heer, E.H. Conrad, C. Berger, Structural properties of the multilayer graphene/4H-SiC(000-1) system as determined by surface x-ray diffraction, Phys. Rev. B 75 (2007) 214109.

[53] P. Thibault, P.M. Guizar-Sicairos, A. Menzel, Coherent imaging at the diffraction limit, J. Synchrotron Radiat. 21 (2014) 1011–1018.

[54] Y. Takahashi,.A. Suzuki, N. Zettsu, Y. Kohmura, Y. Senba, H. Ohashi, Towards high-resolution ptychographic x-ray diffraction microscopy, Phys. Rev. B 83 (2011) 214109.

[55] D.A. Shapiro, Y.-S. Yu, T. Tyliszczak, J. Cabana, R. Celestre, W. Chao, K. Kaznatcheev, A.L.D. Kilcoyne, F. Maia, S. Marchesini, Y.S. Meng, T. Warwick, L.L. Yang, H.A. Padmore, Chemical composition mapping with nanometer resolution by soft X-ray microscopy, Nat. Photonics 8 (2014) 765–769.

[56] M. Holler, A. Diaz, M. Guizar-Sicairos, P. Karvinen, F. Elina, H. Emma, R. Mikko, A. Menzel, J. Raabe, O. Bunk, X-ray ptychographic computed tomography at 16 nm isotropic 3D resolution, Nat. Sci. Rep. 4 (2014) 3857.

[57] Z.H. Zhu, T. Tyliszczak, H.-W. Shiu, D. Shapiro, D.A. Bazylinski, U. Lins, A.P. Hitchcock, Magnetic studies of magnetotactic bacteria by soft X-Ray STXM and ptychography (Proceedings of XRM2014), J. Phys. Conf. Ser. (2015) (in review).

[58] Y. Li, F. El Gabaly, T.R. Ferguson, R.B. Smith, N.C. Bartelt, J.D. Sugar, K.R. Fenton, D.A. Cogswell, A.L.D. Kilcoyne, T. Tyliszczak, M.Z. Bazant, W.C. Chueh,

Current-induced transition from particle-by-particle to concurrent intercalation in phase-separating battery electrodes, Nat. Mater. 13 (2014) 1149–1156.
[59] K.P. Lam, A.P. Hitchcock, M. Obst, J.R. Lawrence, G.D.W. Swerhone, G.G. Leppard, T. Tyliszczak, C. Karunakaran, J. Wang, K. Kaznatcheev, D. Bazylinski, U. Lins, X-ray magnetic circular dichroism of individual magnetosomes by scanning transmission x-ray microscopy, Chem. Geol. 270 (2010) 110–116.
[60] S.S. Kalirai, K.P. Lam, D. Bazylinski, U. Lins, A.P. Hitchcock, Examining the chemistry and magnetism of magnetotactic bacterium Candidatus Magnetovibrio blakemorei strain MV-1 using scanning transmission X-ray microscopy, Chem. Geol. 300–301 (2012) 14–23.
[61] S.S. Kalirai, D.A. Bazylinski, A.P. Hitchcock, Anomalous magnetic orientations of magnetosome chains in a magnetotactic bacterium: Magnetovibrio Blakemorei strain MV-1, Public Libr. Sci. One 8 (2013) 1–7 (e53368).
[62] W. Eberhardt, Synchrotron radiation: a continuing revolution in x-ray science—diffraction limited storage rings and beyond, J. Electron Spectrosc. Relat. Phenom. 200 (2015) 32–40.
[63] M. Eriksson, J.F. van der Veen, C. Quitmann, Diffraction limited storage rings—a window to the science of tomorrow, J. Synchrotron Radiat. 21 (2014) 837–842.
[64] M.D. de Jonge, C.G. Ryan, C.J. Jacobsen, X-ray nanoprobes and diffraction-limited storage rings: opportunities and challenges of fluorescence tomography of biological specimens, J. Synchrotron Radiat. 21 (2014) 1047.
[65] SHARP workshop, Berkeley Lab. ⟨http://camera.lbl.gov/workshops-and-tutorials/sharp-workshop⟩, (accessed 08.10.14).
[66] G.R. Morrison, A. Gianoncelli, B. Kaulich, D. Bacescu, J. Kovac, A fast-readout CCD system for configured-detector imaging in STXM. Proceedings of the 8th International Conference on X-ray Microscopy IPAP Conference 7 (2006) 377–37.
[67] A. Chmyrov, J. Keller, T. Grotjohann, M. Ratz, E. d'Este, S. Jakobs, C. Eggeling, W. Hell, Nanoscopy with more than 100,000 'doughnuts', Nat. Methods 10 (2013) 737–740.
[68] Th. Schmidt, U. Groh, R. Fink, E. Umbach, O. Schaff, W. Engel, B. Richter, H. Kuhlenbeck, R. Schlogl, H.-J. Freund, A.M. Bradshaw, D. Preikszas, P. Hartel, R. Spehr, H. Rose, G. Lilienkamp, E. Bauer, G. Benner, XPEEM with energy-filtering: advantages and first results, Smart Proj. Surf. Rev. Lett. 9 (2002) 223–232.
[69] A. Doran, M. Church, T. Miller, A.T. Young, A. Scholl, Cryogenic PEEM at the advanced light source, J. Electron Spectrosc. Relat. Phenom. 185 (2012) 340–346.
[70] G. Schönhense, K. Medjanik, H.-J. Elmers, Space-, time- and spin-resolved photoemission, J. Electron Spectrosc. 200 (2015) 95–119.
[71] Y. Takeichi, N. Inami, H. Suga, K. Ono, Y. Takahashi, Development of a compact scanning transmission x-ray microscope (STXM) at the photon factory, Chem. Lett. 43 (2014) 373–375.
[72] L.M. Picco, L. Bozec, A. Ulcinas, D.J. Engledew, M. Antognozzi, M.A. Horton, M.J. Miles, Breaking the speed limit with atomic force microscopy, Nanotechnology 18 (2007) 044030.
[73] G. McDermott, M.A. Le Gros, C.G. Knoechel, M. Uchida, C.A. Larabell, Soft x-ray tomography and cryogenic light microscopy: the cool combination in cellular imaging, Trends Cell Biol. 19 (2009) 587–595.
[74] D. Guay, J. Stewart-Ornstein, X. Zhang, A.P. Hitchcock, In situ spatial and time resolved studies of electrochemical reactions by scanning transmission x-ray microscopy, Anal. Chem. 77 (2005) 3479–3487.
[75] L. Bozzini, A. D'Urzo, B. Gianoncelli, M. Kaulich, M. Kiskinova, A. Prasciolu, Tadjeddine, In situ soft x-ray dynamic microscopy of electrochemical processes, Electrochem. Commun. 10 (2008) 1680–1683.
[76] B. Bozzini, M. Amati, A. Gianoncelli, L. Gregoratti, B. Kaulich, M. Kiskinova, New energy sources: in-situ characterisation of fuel cell and supercapacitor components, J. Phys.: Conf. Ser. 463 (2013) 012018.
[77] T. Lefevre, M. Pézolet, D. Hernández Cruz, M.M. West, M. Obst, A.P. Hitchcock, C. Karunakaran, K.V. Kaznatcheev, Mapping molecular orientation in dry and wet dragline spider silk (Proceedings of the 9th International Conference on X-ray Microscopy), J. Phys. Conf. Ser. 186 (2009) 012089.
[78] V. Berejnov, D. Susac, J. Stumper, A.P. Hitchcock, Nano to micro scale characterization of water uptake in the catalyst coated membrane measured by soft x-ray scanning transmission x-ray microscopy, ECS Trans. 41 (2011) 395–402.
[79] S.T. Kelly, P.A. Nigge, S. Prakash, A. Laskin, B. Wang, T. Tyliszczak, S.R. Leone, M.K. Gilles, An environmental sample chamber for reliable scanning transmission x-ray microscopy measurements under water vapor, Rev. Sci. Instrum. 84 (2013) 073708.
[80] E. de Smit, I. Swart, J.F. Creemer, G.H. Hoveling, M.K. Gilles, T. Tyliszczak, P.J. Kooyman, H.W. Zandbergen, C. Morin, B.M. Weckhuysen, F.M.F. de Groot, Nanoscale chemical imaging of a working catalyst by scanning transmission x-ray microscopy, Nature 456 (2008) 226–230.
[81] B. Bozzini, M. Amati, L. Gregoratti, M. Kiskinova, In-situ photoelectron microspectroscopy and imaging of electrochemical processes at the electrodes of a self-driven, Cell Sci. Rep. 3 (2013) 2848.
[82] B. Bozzini, M. Amati, L. Gregoratti, M. Kazemian, M. Prasciolu, E. Tondo, A.L. Trygub, M. Kiskinova, In situ electrochemical x-ray spectromicroscopy investigation of the reduction/reoxidation dynamics of N-Cu solid oxide fuel cell anodic material in contact with a Cr interconnect in 2×10^{-6} mbar O_2, J. Phys. Chem. C 116 (2012) 7243–7248.
[83] A. Kolmakov, D.A. Dikin, L.J. Cote, J. Huang, M. Kazemian Abyaneh, M. Amati, L. Gregoratti, S. Günther, M. Kiskinova, Graphene oxide windows for in situ environmental cell photoelectron spectroscopy, Nat. Nanotechnol. 6 (2011) 651–653.